AUT Journal of Modeling and Simulation

AUT J. Model. Simul., 55(2) (2023) 283-298
DOI: 10.22060/MISCJ.2024.22897.5348

Bernstein-Schurer-Stancu operator–based adaptive controller design for chaos synchronization in the q-analogue

Alireza Izadbakhsh

Department of Electrical Engineering, Garmsar Branch, Islamic Azad University, Garmsar, Iran

ABSTRACT: In this paper, a synchronization controller for chaotic master-slave systems is presented based on the q-analogue of the Bernstein-Schurer-Stancu operators. q-analogue of the Bernstein-Schurer-Stancu operators is employed to approximate uncertainties due to their universal approximation property. The coefficients of polynomials are considered free parameters and will be adjusted by the adaptive rules extracted from the stability analysis. Additionally, the controller is designed based on the presumption that the synchronization error rate is unavailable. The controller is applied on a master-slave system using Duffing-Holmes oscillators. The results are compared with the Radial Basis Function Neural Networks (RBFNN). Simulation results and comparisons show that the Bernstein-Schurer-Stancu operator in q-analogue is efficient in uncertainty approximation; needless, the system states for constructing the regressor vector and can be a good alternative for neural networks.

Review History:

Received: Dec. 28, 2023
Revised: Mar. 06, 2024
Accepted: May, 29, 2024
Available Online: May, 30, 2024

Keywords:

Adaptive Uncertainty Approximation
Neural Network
q-Analogue of the Bernstein-Schurer-Stancu Operators
Synchronization of Chaos
Universal Approximation Theorem

1- Introduction

Chaos is an interesting phenomenon in many real-world systems, from engineering sciences to medical fields. Cryptography and communication systems have witnessed frequent chaos applications (Aliabadi et al., 2022; Razmara & Yahyazadeh, 2022). In power systems, (Abdelmalak et al., 2020; Pinzón & Colomé, 2018; Xu et al., 2018), chaos control is needed, and chaotic signals' prediction is essential. Also, in chemical reactions, chaos occurs (Kol'tsov & Fedotov V K, 2018; Schenkendorf et al., 2019). Various chaotic oscillators are built using nonlinear electrical circuits (Munmuangsaen & Srisuchinwong, 2018; Tian et al., 2019; Zhou et al., 2018). To treat heart issues, cancers, and other diseases, chaos has also been applied (Borah et al., 2021; Gupta et al., 2021; Priyanga et al., 2021).

Since finding two equal oscillators in practice is challenging or impossible, chaos synchronization needs a controller to overcome uncertainties and chaotic dynamics. Besides, the property of totally distinctive responses in the presence of a tiny difference in initial conditions should be emphasized. Therefore, influential adaptive or robust controllers are needed for chaos synchronization, and much research has been reported in this field (Han et al., 2020; Karami et al., 2021; Li et al., 2001; Mobayen & Ma, 2018; Modiri & Mobayen, 2020; Mohammadzadeh et al., 2021; Pal et al., 2021; Wang et al., 2020; Tai et al., 2019; Zhu et al., 2020). Neural networks (Han et al., 2020; Tai et al., 2019) and fuzzy systems (Mohammadzadeh et al., 2021; Zhu et al., 2020) are playing essential roles in many researches as universal approximators. However, as discussed (Izadbakhsh, 2017), many tuning parameters exist in fuzzy or neural controllers.

To solve the issues of neuro-fuzzy systems, less complicated uncertainty approximators using function approximation techniques have been presented (Izadbakhsh, 2018; Izadbakhsh, 2021; Izadbakhsh et al., 2011; Izadbakhsh et al., 2019; Izadbakhsh et al., 2021; Izadbakhsh & Kheirkhahan, 2019; Izadbakhsh & Nikdel, 2021; Izadbakhsh & Rafiei, 2009). Compared to the neuro-fuzzy systems, these approximators (Fourier series expansion, Bernstein polynomials, and differential equations) have less complexity and accompany fewer adjustable parameters. So, tuning the uncertainty approximator is more convenient. It should be noted that the adaptive rules are required for the polynomial coefficients estimation, which is the main difference between this paper in comparison with previous related works on the Bernstein-Schurer-Stancu operators in q-analogue (Büyükyazıcı & Atakut, 2010; Finta & Gupta, 2010). The proposed approximator can approximate the lumped uncertainties, ending good disturbance rejection.

*Corresponding author's email: izadbakhsh_alireza@hotmail.com

The advantage of the Bernstein-Schurer-Stancu operators in q-analogue compared to other universal approximators, such as fuzzy systems and neural networks, are somehow significant. The first subject is that the regressor vector in neural networks and fuzzy systems depends on the system state variables. Thus, the regressor vector's dimension is considerably large for systems of higher order containing a vast amount of state variables. Accordingly, memory usage is greater in the practical implementation of neuro-fuzzy-based controllers. Furthermore, the sample time required to scan the program inside the microcontroller will be more than usual, causing a delay in the applied control signal and thus losing the state of being stable. However, the performance of the q-analogue Bernstein-Schurer-Stancu operators-based controller is clear of the problem mentioned above since the structure of the regressor vector is state-free. The 2nd one is the number of adjustable parameters in the regressor vectors. In the q-analogue of the Bernstein-Schurer-Stancu operators, the designer faces fewer adjustable parameters compared to neuro-fuzzy systems. For instance, (Sheikhan et al., 2013) proposed an optimization algorithm to gain the RBFNN optimal parameters to synchronize chaos. (Wang et al., 2020) investigated a neuro-fuzzy system for chaos synchronization that suffers from a heavy computational load. The proposed strategy includes three adaptation rules with five membership functions for each state variable. Finally, (Boubellouta et al., 2019) proposed an adaptive fuzzy controller with 18 parameters tuned by trial and error. Hence, to make the superiority of the Bernstein-Schurer-Stancu operators in q-analogue clearer, RBFNN has been chosen for comparison purposes. Besides, these approaches' responses were assessed to eliminate the undesirable effect of significant disturbances.

The motivation for utilizing the function approximation-based method is the notable benefits of these techniques compared to model-free neuro-fuzzy and model-based approaches. These benefits are as follows: (1) Unlike model-based controllers, the function approximation-based methods are not affected by parameter changes and un-modelled dynamics; (2) Unlike fuzzy methods or neural networks, the use of these methods does not require special expertise; (3) On the contrary to the neuro-fuzzy strategies, the number of parameters is limited in function approximation approaches; (4) there is no need for projection algorithms. As a result, the computational load of the system is significantly reduced compared to the neural network and fuzzy methods."

Therefore, in this paper, function approximation is utilized to solve the issue of uncertainties and external disturbances. The different sections of the paper are as follows: Section 2 gives the dynamic equation of the Duffing-Holmes oscillator. Section 3 explains a few necessary concepts about the q-analogue of the Bernstein-Schurer-Stancu operators. Section 4 shows the scenario of the controller design accompanying a stability analysis. The results of numerical simulations are presented in Section 5. In the end, the most dominant conclusions are collected in Section 6.

2- The Duffing-Holmes Dynamic Equation

The master/slave subsystems of the Duffing-Holmes oscillator are described as follows:

$$\begin{aligned}\ddot{y}_m(t) = &-r_{m3}y_m^3(t) - r_{m2}\dot{y}_m(t) \\ &-r_{m1}y_m(t) + r_{m4}\cos(\omega_m t)\end{aligned} \tag{1}$$

$$\begin{aligned}\ddot{y}_s(t) = &-r_{s3}y_s^3(t) - r_{s2}\dot{y}_s(t) - r_{s1}y_s(t) \\ &+ r_{s4}\cos(\omega_s t) + u(t) + d(t)\end{aligned} \tag{2}$$

where $y_s(t)$ and $y_m(t)$ show the outputs of the master's/slave's system, respectively. The parameters of the system are illustrated by r_{mi} and r_{si} for i=1,…, 4, which are assumed to be unknown. The constant parameters ω_s and ω_m, indicate the frequency parameters. Lastly, $u(t) \in \Re$ and $d(t) \in \Re$ show the control input and the external disturbances, respectively. Introduce the error of synchronization as $e(t) = y_s(t) - y_m(t)$. Applying the time derivative for $e(t)$ and utilizing (1) and (2), the representation of the master/slave systems can be illustrated in the error space below.

$$\ddot{e}(t) = \wp(t) + u(t) \tag{3}$$

where

$$\begin{aligned}\wp(t) = &\, r_{m1}y_m(t) - r_{s1}y_s(t) + d(t) \\ &-r_{s2}\dot{y}_s(t) - r_{s3}y_s^3(t) + r_{m3}y_m^3(t) \\ &+r_{m2}\dot{y}_m(t) + r_{s4}\cos(\omega_s t) - r_{m4}\cos(\omega_m t)\end{aligned} \tag{4}$$

shows the nonlinear function of uncertainty. This model will be utilized for future chaos synchronization controller design with only the assumption of synchronization error measurement. In other words, it is presumed that the synchronization error's time derivative is inaccessible.

Remark 1: All uncertainties effects have been considered in equation (4) and are presumed to be unknown, bounded, and continuous. Hence, the proposed controller is model-free.

3- The Bernstein-Schurer-Stancu Operators in q-analogue as the function approximator

Let α, β, and p belong to the set of all non-negative integers $\mathbb{N}^0$ such that $0 \le \alpha \le \beta$, then for any $f \in C[0, p+1]$ and $q \in (0,1)$, the Bernstein-Schurer-Stancu Operators in q-analogue is defined by (Agrawal et al., 2013).

$$S_{\Xi,p}^{\alpha,\beta}(f,q,t) = \sum_{k=0}^{p+\Xi} f\left(\frac{\alpha+[k]_q}{\beta+[\Xi]_q}\right)\begin{bmatrix} p+\Xi \\ k \end{bmatrix}_q (1-t)_q^{\Xi-k+p} t^k, \quad \forall t\in[0,1] \tag{5}$$

where $\begin{bmatrix}\Xi \\ k\end{bmatrix}_q$ indicates the coefficient of the q-binomial, being introduced below,

$$\begin{bmatrix}\Xi \\ k\end{bmatrix}_q = \frac{[\Xi]_q !}{[k]_q ![\Xi-k]_q !} \tag{6}$$

in which k and Ξ are any integers satisfying $0\le k\le\Xi$. The q-factorial is shown by $[k]_q !$ and is expressed as

$$[k]_q ! = \begin{cases} 1 & k=0 \\ [k]_q [k-1]_q \ldots 1 & k\ge 1 \end{cases} \tag{7}$$

in which

$$[k]_q = \begin{cases} \dfrac{(1-q^k)}{(1-q)}, & q\ne 1 \\ k & q=1 \end{cases} \tag{8}$$

denotes the q-integer of the number $k\in\mathbb{N}$. Considering Theorem 1 of (Agrawal et al., 2013), concerning any function $f\in C[0,p+1]$ and $q\in(0,1)$, it has been shown that $S_{\Xi,p}^{\alpha,\beta}(f,q,t)$ converges to $f(t)$ uniformly on the interval $[0,1]$. It is not difficult to show that:

$$S_{\Xi,p}^{\alpha,\beta}(f,q,t) = \mathbf{\Lambda}_f^T \boldsymbol{\xi}_f \tag{9}$$

where

$$\mathbf{\Lambda}_f = [f\left(\frac{\alpha}{\beta+[\Xi]_q}\right) \quad [p+\Xi]_q f\left(\frac{\alpha+1}{\beta+[\Xi]_q}\right) \quad \ldots \quad f\left(\frac{\alpha+[p+\Xi]_q}{\beta+[\Xi]_q}\right)]^T \in \Re^{p+\Xi+1} \tag{10}$$

is a vector containing adjustable parameters and

$$\boldsymbol{\xi}_f = \left[(1-t)_q^{p+\Xi} \quad (1-t)_q^{p+\Xi-1} t \quad \ldots \quad t^{p+\Xi}\right]^T \in \Re^{p+\Xi+1} \tag{11}$$

is the basis functions' vector. Equation (5) can be represented as equation (9), a standard format in adaptive control.

Remark 2: The finite term of the *Bernstein-Schurer-Stancu operator* in *q-analogue* (5) is utilized for approximations of functions, and residual terms are assumed as the truncation error.

4- Proposed approach

Applying the Bernstein-Schurer-Stancu operator in q-analogue as the uncertainty approximator and using only synchronization error measurement, an adaptive control strategy is suggested for chaos synchronization. In other words, there is no knowledge of $\dot{e}(t)$. Toward this aim, we propose the following control input:

$$u(t) = -\kappa_2\gamma^2 e(t) - \kappa_1\gamma^2\omega(t) - \hat{\wp}(t) \tag{12}$$

where $\omega(t)\in\Re$ is an auxiliary variable that will be defined later (in Eq. (26)), κ_1 and κ_2 are positive scalar constants, γ is a positive scalar constant chosen large enough, and $\hat{\wp}(t)$ is an approximation of $\wp(t)$. Substituting (12) into (3), we have

$$\ddot{e}(t) = \wp(t) - \hat{\wp}(t) - \kappa_1\gamma^2\omega(t) - \kappa_2\gamma^2 e(t) \tag{13}$$

If some suitable adaption rule can be found in such a way that $\hat{\wp}(t) = \wp(t) + \varepsilon_\wp$, the uniform boundedness of $e(t)$ and $\dot{e}(t)$ is then guaranteed from equation (13). To this mean, it is assumed that there exists a Bernstein-Schurer-Stancu operator in q-analogue that approximates $\wp(t)$ as

$$\wp(t) = \mathbf{\Lambda}^T \boldsymbol{\xi} + \varepsilon_\wp \tag{14}$$

where $\ddot{\mathbf{E}}\in\Re^{(N+1)}$ is the actual system parameters' constant vector, N is the number of basis functions, and $\varepsilon_\wp\in\Re$ explains the bounded approximation error. Making use of a similar number of basis functions, we have also:

$$\hat{\wp}(t) = \hat{\mathbf{\Lambda}}^T \boldsymbol{\xi} \tag{15}$$

where $\hat{\mathbf{E}}\in\Re^{(N+1)}$ is an estimate of $\ddot{\mathbf{E}}$. Now, substituting (14) and (15) into (13) obtains

$$\ddot{e}(t) = \tilde{\mathbf{\Lambda}}^T \boldsymbol{\xi} + \varepsilon_{\wp} - \kappa_1 \gamma^2 \omega(t) - \kappa_2 \gamma^2 e(t) \tag{16}$$

where $\tilde{\ddot{\mathbf{E}}} = \ddot{\mathbf{E}} - \hat{\mathbf{E}} \in \Re^{(N+1)}$ describe the coefficients' error vector related to the Bernstein-Schurer-Stancu operator in q-analogue.

4- 1- Analysis of the stability

Before starting the analysis of the stability, we present the following lemma.

Lemma1: Consider the coupled dynamical system $\dot{\mathbf{z}}_1 = \mathbf{f}_1(\mathbf{z}_1, \mathbf{z}_2, t)$ and $\dot{\mathbf{z}}_2 = \mathbf{f}_2(\mathbf{z}_1, \mathbf{z}_2, t)$. Let the positive definite function $V(\mathbf{z}_1, \mathbf{z}_2, t)$ has the following features:

$$\alpha_1 \|\mathbf{z}_1\|^2 + \alpha_2 \|\mathbf{z}_2\|^2 \le V \le \alpha_3 \|\mathbf{z}_1\|^2 + \alpha_4 \|\mathbf{z}_2\|^2 \tag{17}$$

$$\dot{V} \le -\alpha_5 \|\mathbf{z}_1\|^2 - \alpha_6 \|\mathbf{z}_2\|^2 + \varphi \tag{18}$$

where φ and α_i are positive scalar constants. Determine $\delta = \max(\alpha_3/\alpha_5, \alpha_4/\alpha_6)$ and $\Im_i = \sqrt{\delta\varphi/\alpha_i}$ for i=1,2. As a result, $\mathbf{z}_1(t)$ and $\mathbf{z}_2(t)$ will be uniformly bounded for any initial system states' $\mathbf{z}_1(0)$ and $\mathbf{z}_2(0)$; and will converge exponentially to the closed balls $B_{\Im_1}$, $B_{\Im_2}$, respectively, where $B_{\Im_i} = \{\mathbf{z}_i : |\mathbf{z}_i| \le \Im_i\}$. Further details can be found in (Colbaugh et al., 1995). **Proof:** The direct application of Corless's Theorem on global exponential convergence (Corless, 1990) yields the result.

The main results of the proposed scheme are summarized in the following Theorem.

Theorem 1: Consider the dynamic equation (3) along with the control law (12) and the adaptation law (27). By selecting an appropriate number of q-analogue Bernstein-Schurer-Stancu operators and applying Lemma 1, it is established that both $\|\mathbf{z}\|$ and $\|\tilde{\mathbf{E}}\|$ remain uniformly bounded and converge exponentially to a closed ball.

Proof: Consider the following positive-definite function.

$$\begin{aligned} V(e, \dot{e}, \omega, \tilde{\mathbf{\Lambda}}) &= \frac{1}{2}\kappa_2 \gamma^2 e^2 + \frac{1}{2}\dot{e}^2 + \frac{1}{2}\kappa_1 \omega^2 \\ &+ \frac{\kappa_2}{\kappa_1 \gamma} e\dot{e} - \frac{1}{\gamma}\omega\dot{e} + \frac{1}{2}\tilde{\mathbf{\Lambda}}^T \mathbf{Q} \tilde{\mathbf{\Lambda}} \end{aligned} \tag{19}$$

where $\mathbf{Q} \in \Re^{(N+1)\times(N+1)}$ is a positive diagonal gain matrix. Note that $V(e, \dot{e}, \omega, \tilde{\mathbf{E}})$ is radially unbounded and the positive-definite of the closed-loop system state if γ is chosen large enough.

The time derivative of (19) is obtained as

$$\begin{aligned} \dot{V}(e, \dot{e}, \omega, \tilde{\mathbf{\Lambda}}) &= \rho(t)\ddot{e} + \kappa_1 \omega\dot{\omega} \\ &+ \kappa_2 \gamma^2 e\dot{e} + \frac{\kappa_2}{\kappa_1 \gamma}\dot{e}^2 - \frac{1}{\gamma}\dot{\omega}\dot{e} - \tilde{\mathbf{\Lambda}}^T \mathbf{Q} \dot{\hat{\mathbf{\Lambda}}} \end{aligned} \tag{20}$$

where

$$\rho(t) = \frac{\kappa_2}{\kappa_1 \gamma} e(t) - \frac{1}{\gamma}\omega(t) + \dot{e}(t) \tag{21}$$

Substituting (16) into (20) results in:

$$\begin{aligned} \dot{V}(e, \dot{e}, \omega, \tilde{\mathbf{\Lambda}}) &= \rho(t)(-\kappa_1 \gamma^2 \omega - \kappa_2 \gamma^2 e + \tilde{\mathbf{\Lambda}}^T \boldsymbol{\xi} + \varepsilon_{\wp}) \\ &+ \kappa_2 \gamma^2 e\dot{e} + \kappa_1 \omega\dot{\omega} + \frac{\kappa_2}{\kappa_1 \gamma}\dot{e}^2 \\ &- \frac{1}{\gamma}\dot{\omega}\dot{e} - \tilde{\mathbf{\Lambda}}^T \mathbf{Q} \dot{\hat{\mathbf{\Lambda}}} \end{aligned} \tag{22}$$

That can be simplified as:

$$\begin{aligned} \dot{V}(e, \dot{e}, \omega, \tilde{\mathbf{\Lambda}}) &= -\rho(t)(\kappa_1 \gamma^2 \omega + \kappa_2 \gamma^2 e) \\ &+ \rho(t)\varepsilon_{\wp} + \kappa_2 \gamma^2 e\dot{e} + \kappa_1 \omega\dot{\omega} + \frac{\kappa_2}{\kappa_1 \gamma}\dot{e}^2 \\ &- \frac{1}{\gamma}\dot{\omega}\dot{e} - \tilde{\mathbf{\Lambda}}^T (\mathbf{Q}\dot{\hat{\mathbf{\Lambda}}} - \boldsymbol{\xi}(t)\rho(t)) \end{aligned} \tag{23}$$

Substituting (21) into (23) gives:

$$\begin{aligned} \dot{V}(e, \dot{e}, \omega, \tilde{\mathbf{\Lambda}}) &= -\kappa_1 \gamma^2 \dot{e}\omega - \frac{\kappa_2^2}{\kappa_1}\gamma e^2 \\ &+ \kappa_1 \gamma \omega^2 + \rho\varepsilon_{\wp} + \kappa_1 \omega\dot{\omega} + \frac{\kappa_2}{\kappa_1 \gamma}\dot{e}^2 \\ &- \frac{1}{\gamma}\dot{\omega}\dot{e} - \tilde{\mathbf{\Lambda}}^T (\mathbf{Q}\dot{\hat{\mathbf{\Lambda}}} - \boldsymbol{\xi}(t)\rho(t)) \end{aligned} \tag{24}$$

Adding and subtracting $\kappa_1 \gamma \omega^2$ to the right-hand side of (24), and some simplification, yields:

$$\dot{V}(e,\dot{e},\omega,\tilde{\mathbf{\Lambda}}) = (-\kappa_1\gamma^2\dot{e} + \kappa_1\dot{\omega} + 2\kappa_1\gamma\omega)\omega -\kappa_1\gamma\omega^2 - \frac{\kappa_2^2}{\kappa_1}\gamma e^2 + \rho\varepsilon_{\wp} - \frac{1}{\gamma}\dot{\omega}\dot{e} + \frac{\kappa_2}{\kappa_1\gamma}\dot{e}^2 - \tilde{\mathbf{\Lambda}}^T(\mathbf{Q}\dot{\hat{\mathbf{\Lambda}}} - \xi(t)\rho(t)) \tag{25}$$

By setting

$$\dot{\omega} = -2\gamma\omega + \gamma^2\dot{e} \tag{26}$$

and

$$\dot{\hat{\mathbf{\Lambda}}} = \mathbf{Q}^{-1}(\xi(t)\rho(t) - \sigma\hat{\mathbf{\Lambda}}) \tag{27}$$

One can write Eq. (25) as follows:

$$\dot{V}(e,\dot{e},\omega,\tilde{\mathbf{\Lambda}}) = -\frac{\kappa_2^2}{\kappa_1}\gamma e^2 - \kappa_1\gamma\omega^2 + \rho\varepsilon_{\wp} + \frac{\kappa_2}{\kappa_1\gamma}\dot{e}^2 - \frac{1}{\gamma}\dot{\omega}\dot{e} + \sigma\tilde{\mathbf{\Lambda}}^T\hat{\mathbf{\Lambda}} \tag{28}$$

Now, substituting (26) into (28) results in the following inequality:

$$\begin{aligned}\dot{V}(e,\dot{e},\omega,\tilde{\mathbf{\Lambda}}) &= -\frac{\kappa_2^2}{\kappa_1}\gamma e^2 - \kappa_1\gamma\omega^2 + \rho\varepsilon_{\wp} - (\gamma - \frac{\kappa_2}{\kappa_1\gamma})\dot{e}^2 + 2\omega\dot{e} + \sigma\tilde{\mathbf{\Lambda}}^T\hat{\mathbf{\Lambda}} \\ &\le -\frac{\kappa_2^2}{\kappa_1}\gamma|e|^2 - (\gamma - \frac{\kappa_2}{\kappa_1\gamma})|\dot{e}|^2 - \kappa_1\gamma|\omega|^2 + |\rho||\varepsilon_{\wp}| + 2|\omega||\dot{e}| + \sigma(\tilde{\mathbf{\Lambda}}^T\mathbf{\Lambda} - \|\tilde{\mathbf{\Lambda}}\|^2)\end{aligned} \tag{29}$$

Now, introducing

$$\mathbf{z} = \begin{bmatrix}|e| & |\dot{e}| & |\omega|\end{bmatrix}^T \tag{30}$$

Equation (29) can be rewritten as follows:

$$\dot{V}(\mathbf{z},\tilde{\mathbf{\Lambda}}) \le |\rho||\varepsilon_{\wp}| - \lambda_{\min}(\mathbf{Q}^*)\|\mathbf{z}\|^2 + \sigma(\tilde{\mathbf{\Lambda}}^T\mathbf{\Lambda} - \|\tilde{\mathbf{\Lambda}}\|^2) \tag{31}$$

where

$$\mathbf{Q}^* = \begin{bmatrix} \frac{\kappa_2^2}{\kappa_1}\gamma & 0 & 0 \\ 0 & (\gamma - \frac{\kappa_2}{\kappa_1\gamma}) & 1 \\ 0 & 1 & \kappa_1\gamma \end{bmatrix} \in \Re^{3\times 3} \tag{32}$$

is positive definite for any large enough chosen γ.

Result 1: Assume that a suitable value is selected for N so that the resulting approximation error is negligible. Hence, (31) is rewritten as

$$\dot{V}(\mathbf{z},\tilde{\mathbf{\Lambda}}) \le -\lambda_{\min}(\mathbf{Q}^*)\|\mathbf{z}\|^2 \tag{33}$$

Consequently, it is confirmed that $\mathbf{z}$ asymptotically converges to zero, using Barbalat's Lemma.

Result 2: With the existence of the approximation error and the σ-modification terms, equation (31) may not conclude its definiteness as the one we have in (33). It is not hard to show that

$$|\rho||\varepsilon_{\wp}| - \lambda_{\min}(\mathbf{Q}^*)\|\mathbf{z}\|^2 \le \frac{9}{2}\frac{|\varepsilon_{\wp}|^2}{\lambda_{\min}(\mathbf{Q}^*)} - \frac{1}{2}\lambda_{\min}(\mathbf{Q}^*)\|\mathbf{z}\|^2 \tag{34}$$

$$\tilde{\mathbf{\Lambda}}^T\mathbf{\Lambda} - \|\tilde{\mathbf{\Lambda}}\|^2 \le \frac{1}{2}(\|\mathbf{\Lambda}\|^2 - \|\tilde{\mathbf{\Lambda}}\|^2) \tag{35}$$

where we utilized the fact that $|\rho| \le 3\|\mathbf{z}\|$, which $\|\bullet\|$ indicates the Euclidian norm. Therefore (31) becomes

$$\dot{V}(\mathbf{z},\tilde{\mathbf{\Lambda}}) \le -\frac{\sigma}{2}\|\tilde{\mathbf{\Lambda}}\|^2 - \frac{1}{2}\lambda_{\min}(\mathbf{Q}^*)\|\mathbf{z}\|^2 + \frac{\sigma}{2}\|\mathbf{\Lambda}\|^2 + \frac{9}{2}\frac{|\varepsilon_{\wp}|^2}{\lambda_{\min}(\mathbf{Q}^*)} \tag{36}$$

Consider the upper/lower bound of (19) as follows:

$$\frac{1}{2}\lambda_{\min}(\mathbf{Q})\left\|\tilde{\mathbf{\Lambda}}\right\|^2+\lambda_{\min}(\mathbf{Q}^*)\left\|\mathbf{z}\right\|^2\le$$
$$V(\mathbf{z},\tilde{\mathbf{\Lambda}})\le\frac{1}{2}\lambda_{\max}(\mathbf{Q})\left\|\tilde{\mathbf{\Lambda}}\right\|^2+\lambda_{\max}(\mathbf{Q}^*)\left\|\mathbf{z}\right\|^2 \quad (37)$$

where

$$\mathbf{Q}^*=\frac{1}{2}\begin{bmatrix}\kappa_2\gamma^2 & \frac{\kappa_2}{\kappa_1\gamma} & 0\\ \frac{\kappa_2}{\kappa_1\gamma} & 1 & \frac{-1}{\gamma}\\ 0 & \frac{-1}{\gamma} & \kappa_1\end{bmatrix} \quad (38)$$

will be positive definite choosing γ large enough. Lemma 1 now is utilized for (36) and (37). It allows that $\|\mathbf{z}\|$ and $\|\tilde{\mathbf{E}}\|$ be uniformly bounded, which also implies uniform boundedness of e , $\dot{e}$, ω and $\hat{\mathbf{E}}$. Furthermore, exponential convergence of $\|\mathbf{z}\|$ and $\|\tilde{\mathbf{E}}\|$ to the closed balls $B_{\Im_1}$, $B_{\Im_2}$, respectively, is guaranteed where

$\delta=\max\left(\frac{2\lambda_{\max}(\mathbf{Q}^*)}{\lambda_{\min}(\mathbf{Q}^*)},\frac{\lambda_{\max}(\mathbf{Q})}{\sigma}\right)$, $\Im_1=\sqrt{\frac{\delta}{\lambda_{\min}(\mathbf{Q}^*)}\left(\frac{9}{2}\frac{|\varepsilon_{\wp}|^2}{\lambda_{\min}(\mathbf{Q}^*)}+\frac{\sigma}{2}\|\ddot{\mathbf{E}}\|^2\right)}$

and $\Im_2=\sqrt{\frac{2\delta}{\lambda_{\min}(\mathbf{Q})}\left(\frac{9}{2}\frac{|\varepsilon_{\wp}|^2}{\lambda_{\min}(\mathbf{Q}^*)}+\frac{\sigma}{2}\|\ddot{\mathbf{E}}\|^2\right)}$.

5- Simulation

The numerical simulations for chaos synchronization problems of two Duffing-Holmes oscillators mentioned in equations (1) and (2) with mismatched parameters are presented in this section. The parameters of the actual values for simulation are $(r_{m1},r_{m2},r_{m3},r_{m4},\omega_m)=(-3,0.4,1,2,2)$ and $(r_{s1},r_{s2},r_{s3},r_{s4},\omega_s)=(-1.2,0.3,1.4,3.9,0.5)$. It is presumed that there exists a 10% parametric variation in the system parameters. The master/slave systems' initial conditions are set to $\begin{bmatrix}y_m(0) & \dot{y}_m(0)\end{bmatrix}=\begin{bmatrix}1 & 0\end{bmatrix}$ and $\begin{bmatrix}y_s(0) & \dot{y}_s(0)\end{bmatrix}=\begin{bmatrix}0 & 0\end{bmatrix}$, respectively.

Test 1:

To assess the efficiency of the suggested strategy, this controller is used for the master/slave system, and the outcomes are shown. Suppose that $\kappa_1=\kappa_2=1$, and $\gamma=5$. The first six terms of the Bernstein-Schurer-Stancu operator in *q*-analogue are utilized as the regressor vector's basis functions for uncertainty compensation. Thus $\hat{\mathbf{E}}$ belongs to $\Re^6$. Random values have been set as initial amounts for the estimated parameters and $\mathbf{Q}=2\times10^{-6}\mathbf{I}_6$ which $\mathbf{I}_6$ denotes a 6×6 identity matrix.

The performance of the suggested *q*-analogue of the Bernstein-Schurer-Stancu operator-based controller in comparison with another existing approximator (Izadbakhsh et al., 2021) is also presented. According to (Izadbakhsh et al., 2021), we obtain

$$\dot{\hat{\mathbf{e}}}(t)=\mathbf{L}'\mathbf{c}_1^T\tilde{\mathbf{e}}(t)+\hat{\wp}(t)+\mathbf{F}\hat{\mathbf{e}}(t)+\mathbf{G}u(t) \quad (39)$$

$$u(t)=-\hat{\wp}(t)-\mathbf{K}\hat{\mathbf{e}}(t) \quad (40)$$

where

$$\mathbf{e}=\begin{bmatrix}y_s(t)-y_m(t)\\ \dot{y}_s(t)-\dot{y}_m(t)\end{bmatrix}\in\Re^2,\ \mathbf{F}=\begin{bmatrix}0&1\\0&0\end{bmatrix}\in\Re^{2\times2},$$
$$\mathbf{G}=\begin{bmatrix}0\\1\end{bmatrix}\in\Re^2,\ \mathbf{c}_1=\begin{bmatrix}1&0\end{bmatrix}^T\in\Re^2 \quad (41)$$

in which $\mathbf{L}'=\begin{bmatrix}l_1 & l_2\end{bmatrix}^T$ and $\mathbf{K}$ are the gain matrices used in the observer and controller, respectively. The term $\hat{\wp}(t)$ is an estimation of $\wp(t)$ in (4), calculated by RBFNN in the form of:

$$\hat{\wp}(t)=\hat{\mathbf{\Lambda}}_o^T\boldsymbol{\xi}_o \quad (42)$$

where $\hat{\mathbf{E}}_o\in\Re^{N_o+1}$ is the weight vector of RBFNN updated by the adaptive law:

$$\dot{\hat{\mathbf{\Lambda}}}_o=\mathbf{\Gamma}_o^{-1}(\boldsymbol{\xi}_o\mathbf{c}_1^T\tilde{\mathbf{e}}(t)-\sigma_o\hat{\mathbf{\Lambda}}_o) \quad (43)$$

where σ_o is a positive constant, $\tilde{\mathbf{\Lambda}}_o\in\Re^{(N_o+1)\times(N_o+1)}$ is the matrix of convergence rate, and N_o indicates the number of the basis functions. The term $\hat{\mathbf{1}}_o$ is the activation function vector used in RBFNN. It should be mentioned that Gaussian functions are used in the RBFNN in this simulation. Suppose that the elements of the vector $\hat{\mathbf{e}}(t)$ are applied at the inputs of RBFNN. As a result,

$$\boldsymbol{\xi}_o=\begin{bmatrix}\xi_1 & \xi_2 & \dots & \xi_{N_o+1}\end{bmatrix}^T\in\Re^{(N_o+1)} \quad (44)$$

$$\xi_i=\exp\left(-\frac{\|\hat{\mathbf{e}}(t)-\mathbf{c}_i\|^2}{\delta_i^2}\right)\quad i=1,2,\dots,N_o+1 \quad (45)$$

Consider $\mathbf{K}=[2\quad 3]$, $\tilde{\mathbf{\Lambda}}_o=2\times10^{-8}\mathbf{I}_6$ and $\mathbf{L}'=[2\quad 10^3]^T\times10^3$. The values of $\mathbf{c}_i$ and δ_i are set to

Table 1. The essential feedback and learning parameters for all approaches

	Learning rate matrix	The required states for function approximation
The proposed approach	$\mathbf{Q} = 2\times10^{-6}\mathbf{I}_6$ and q	Regressor free
RBFNN	$\mathbf{Q} = 2\times10^{-6}\mathbf{I}_6$, $\mathbf{c}_1$, and δ_i for i=1,2,…,6	e and $\dot{e}$ or their estimation

$$\mathbf{c}_1 = \begin{bmatrix} -2\times10^{-2} \\ -4.5 \end{bmatrix}, \mathbf{c}_2 = \begin{bmatrix} -1.6\times10^{-3} \\ -3.6 \end{bmatrix},$$
$$\mathbf{c}_3 = \begin{bmatrix} -1.2\times10^{-3} \\ -2.7 \end{bmatrix}, \mathbf{c}_4 = \begin{bmatrix} -8\times10^{-3} \\ -1.8 \end{bmatrix} \quad (46)$$
$$\mathbf{c}_5 = \begin{bmatrix} -4\times10^{-2} \\ -0.9 \end{bmatrix}, \quad \mathbf{c}_6 = \begin{bmatrix} 0 \\ 0 \end{bmatrix}$$

$$\delta_1 = 4,\ \delta_2 = 3,\ \delta_3 = 2,\ \delta_4 = 2,\ \delta_5 = 1,\ \delta_6 = 0.5 \quad (47)$$

These values have been obtained by trial and error and not optimally. Yet, a satisfactory response is achieved using these values. Also, we suppose that $d(t) = 0.2sin(10t)$. Table 1 outlines the essential feedback and learning parameters for executing two methods.

Based on the above-mentioned parameter settings, the responses are shown in Figs. 1 to 6. Fig. 1 presents the profiles of state variables and influences of both approaches in chaos synchronization. The responses for the case in which no control input is applied are also presented in this Figure. According to this Figure, both approaches perform similarly in the steady state. The significant issue is that the designer is involved in more tuning coefficients in RBFNN (such as $\mathbf{c}_i$ and δ_i) to construct the regressor vector, and finding the best values for them is difficult. Furthermore, RBFNN needs all the arguments of the estimated function, while the Bernstein-Schurer-Stancu operator in q-analogue is free from these arguments. Therefore, in control of systems with large amounts of state variables as the arguments of the lumped uncertainty, the regressor vector in RBFNN is a high-dimension vector. Therefore, from the viewpoint of computational load and memory usage, the Bernstein-Schurer-Stancu operator-based controller in q-analogue is superior to RBFNN. Fig. 2 presents the related synchronization errors. Fig. 3 shows the state error trajectory. The controller output is shown in Fig. 4. As seen in this Figure, this signal is bounded and smooth. The performances of the RBFNN and the proposed method in approximating $\wp(t)$ are shown in Fig. 5. Finally, the related approximation errors are presented in Fig. 6.

To compare the results numerically, consider the following criterion:

$$J_e = \frac{1}{40}\int_0^{40} \left| y_s(t) - y_m(t) \right| dt \quad (48)$$

For the Bernstein-Schurer-Stancu operator in q-analogue, we will have $J_e = 0.06331$, and for the controller based on uncertainty approximation using RBFNN, we have $J_e = 0.04684$.

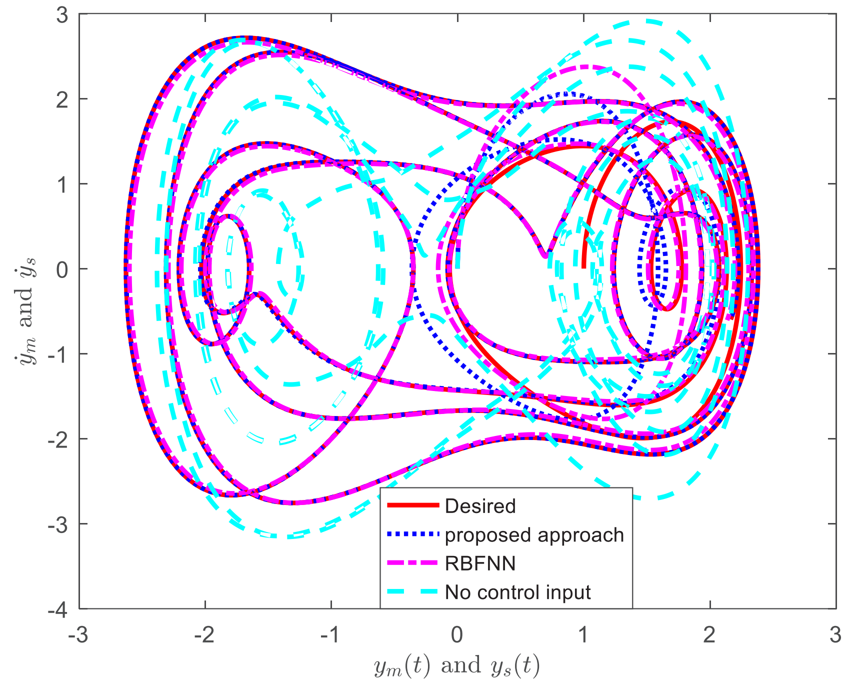

Fig. 1. The synchronization performance

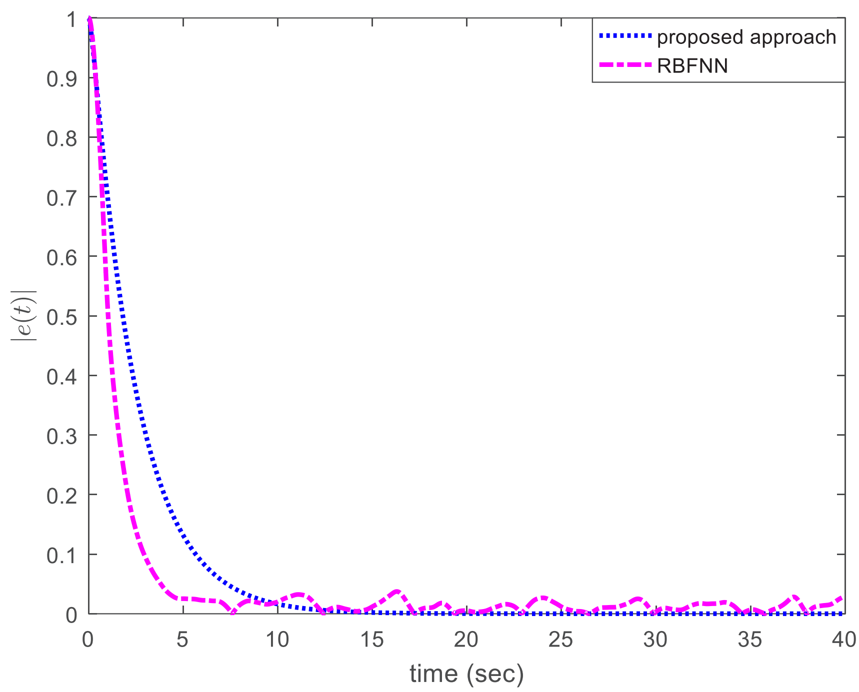

Fig. 2. The synchronization errors

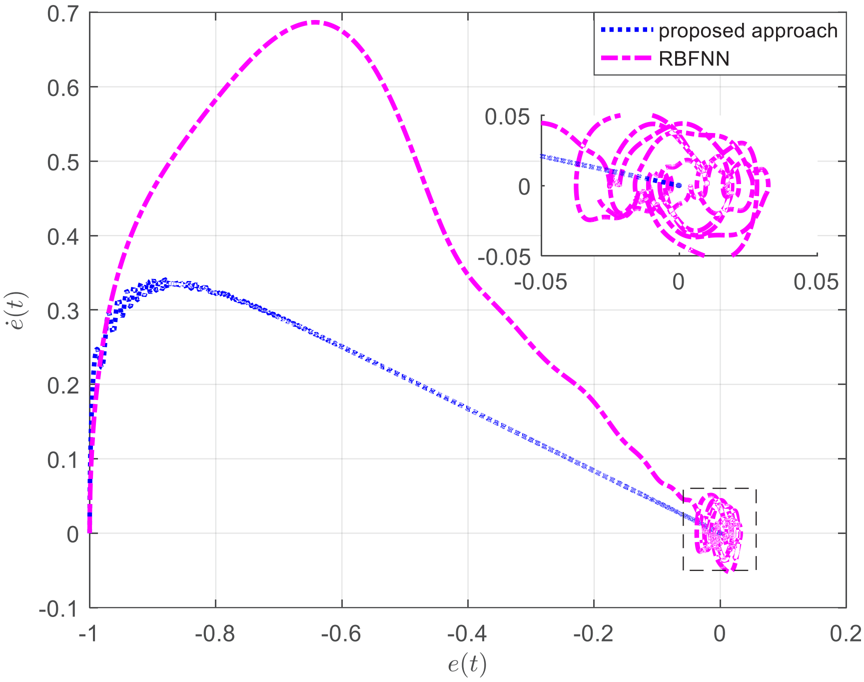

Fig. 3. The state error trajectory

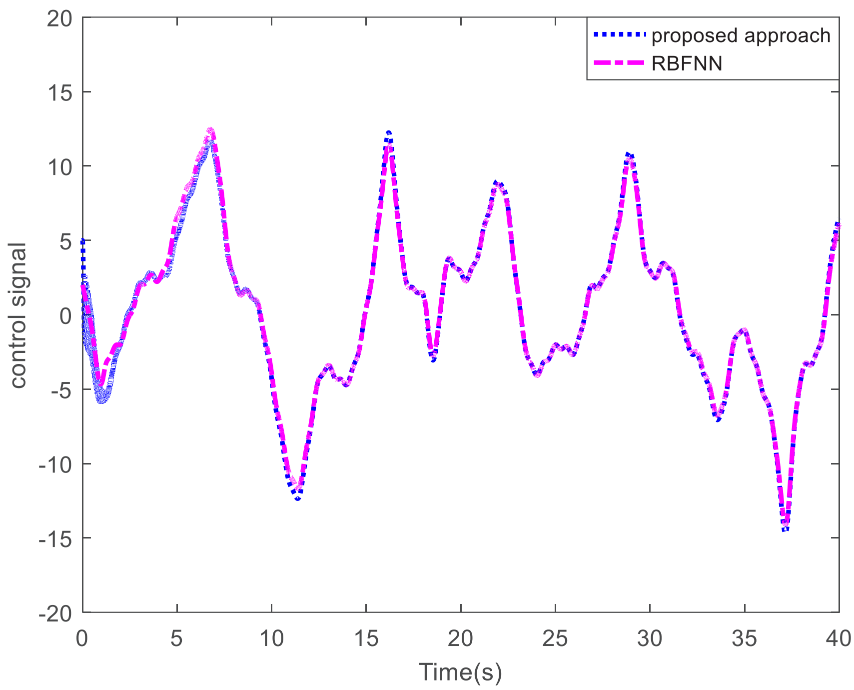

Fig. 4. The control signal

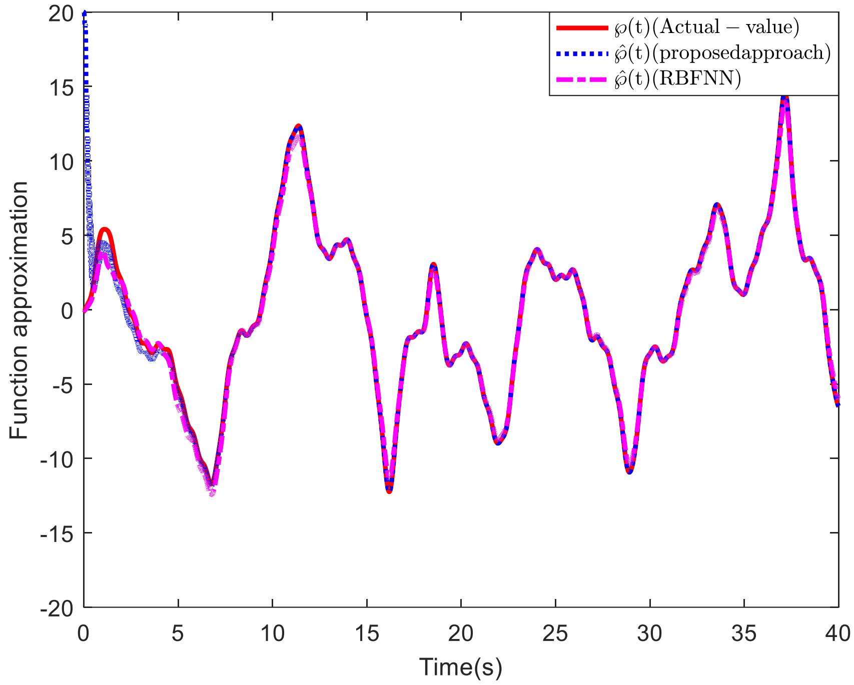

Fig. 5. Approximation of $\wp(t)$

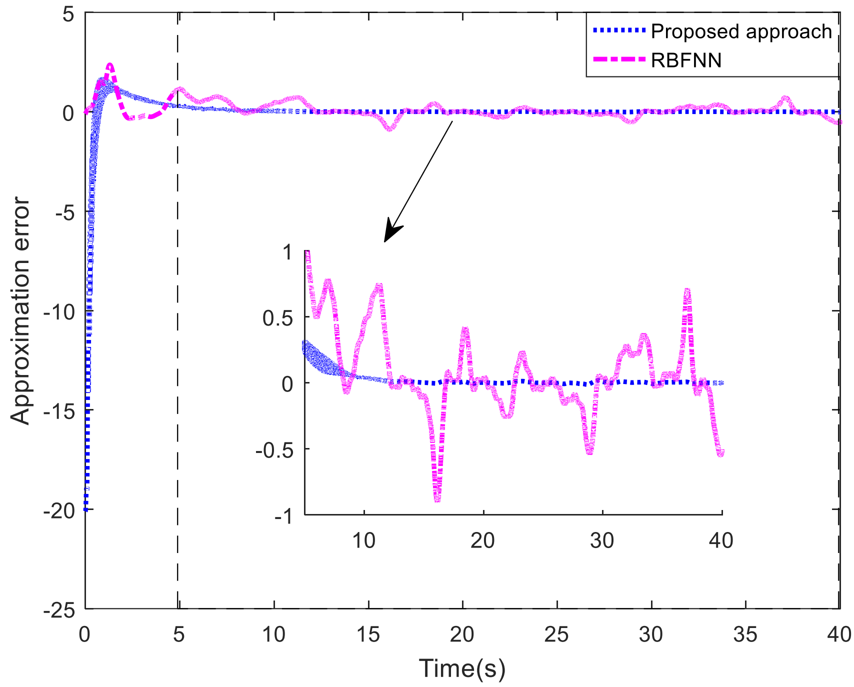

Fig. 6. The related approximation errors

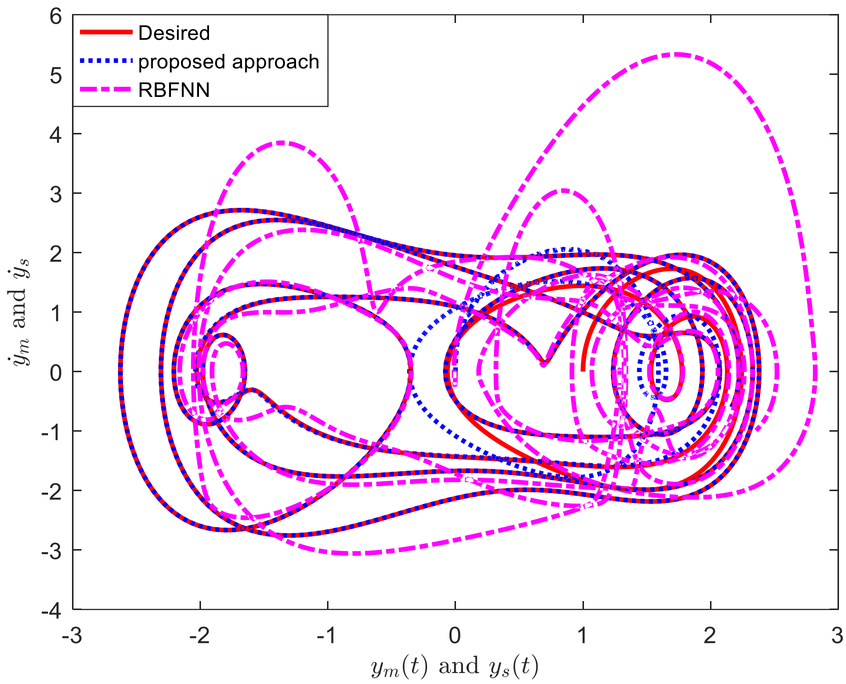

Fig. 7. The synchronization assessment facing external disturbance in (49)

Test 2:

The following external disturbance is applied to the system.

$$d(t) = 12\sin(5t + 5.43) + 12\sin(3.5t - 1.57) \quad (49)$$

To assess the synchronization performance of the RBFNN and q-analogue of the Bernstein-Schurer-Stancu operator, consider Fig. 7 under the same control setting as before. As can be seen, RBFNN has not received a good response. Fig. 8 presents the related synchronization errors. Fig. 9 shows the error trajectory in the state space. The output of the controllers is plotted in Fig. 10. As shown in Fig. 10, these signals are bounded and smooth, lacking the chattering problem. In the end, the uncertainty approximation's performance is shown in Fig. 11.

To compare the results numerically, consider the criterion (48). For the Bernstein-Schurer-Stancu operator in q-analogue, we will have $J_e = 0.06613$, and for the controller based on uncertainty approximation using RBFNN, we have $J_e = 0.2623$ that implies 75% improvement. Optimization algorithms such as particle swarm optimization or genetic algorithm can enhance the controller's accuracy based on RBFNN. However, this task is time-consuming and cannot be performed when the system is affected by external disturbance. This comparison showed that the proposed Bernstein-Schurer-Stancu operator-based approach in q-analogue is more user-friendly and can result in more accurate responses with fewer tuning parameters and less computational burden.

6- Conclusion

A chaos synchronization controller has been proposed by applying the Bernstein-Schurer-Stancu operator in q-analogue. Considering the presumption that the synchronization error is the only measurable state, the proposed control scheme has been introduced. Also, it has been assumed that the chaotic systems' mathematical models are unknown. Many former research studies have used the Bernstein-Schurer-Stancu operators in q-analogue for function approximation. However, this paper has thoroughly developed a different application for these operators. The initiation of this main difference derives from the fact that the function that should be approximated is considered wholly known in the usual function approximation problem. In contrast, this function is uncertain in control systems engineering. The stability analysis used the Lyapunov theorem to extract the adaption law and guarantee a satisfactory controller response. The outcomes are also compared to some different approximators. In future works, the q-analogue of the Bernstein-Schurer-Stancu operators can be developed for communication systems in which chaotic signals are required. Besides, the suggested controller can be appropriate for cooperative or

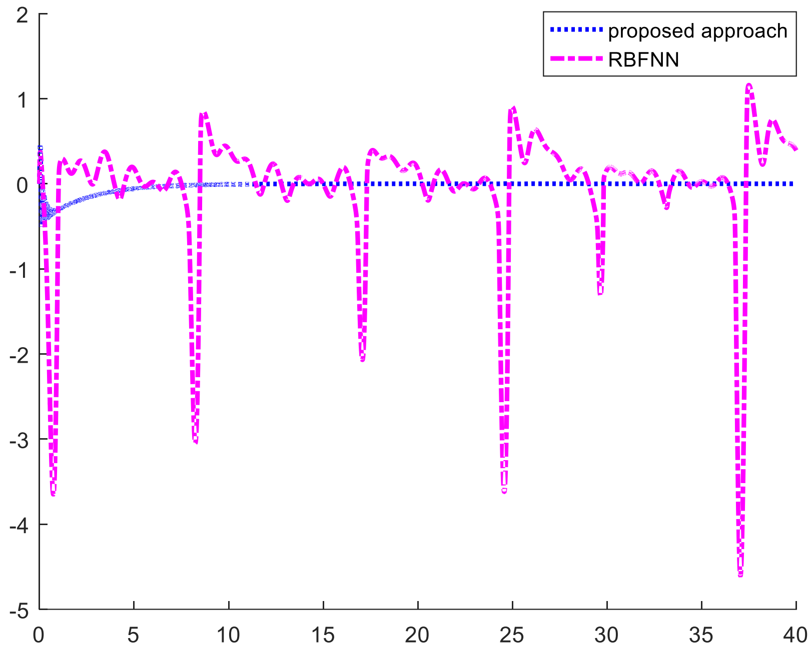

Fig. 8. The synchronization errors

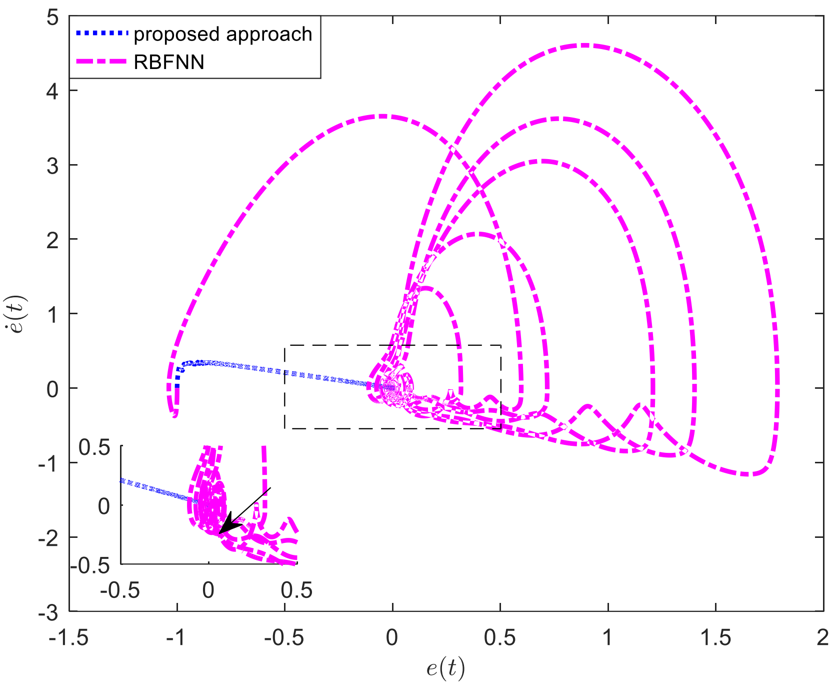

Fig. 9.The state error trajectory in Test 2

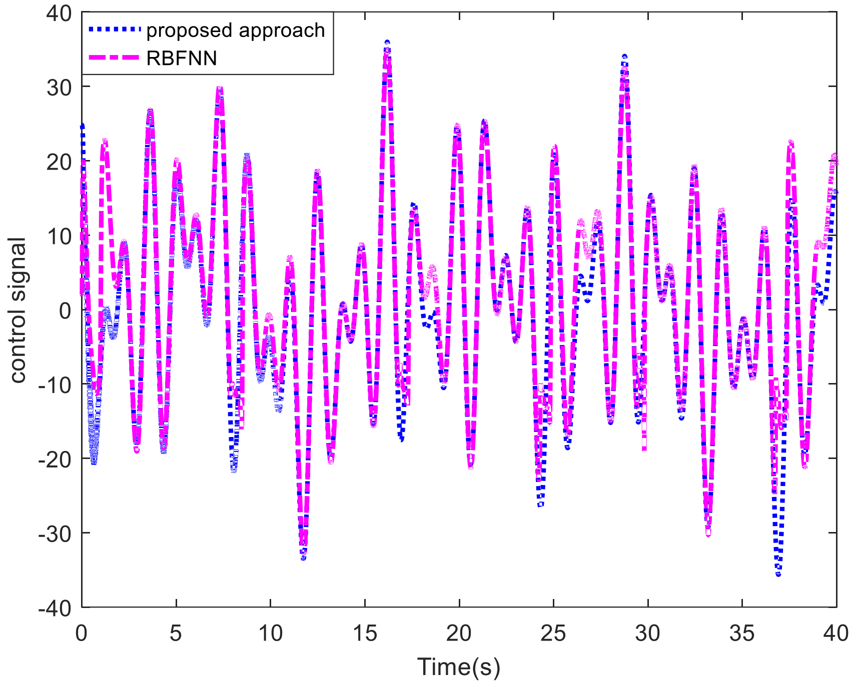

Fig. 10. The control signals in Test 2

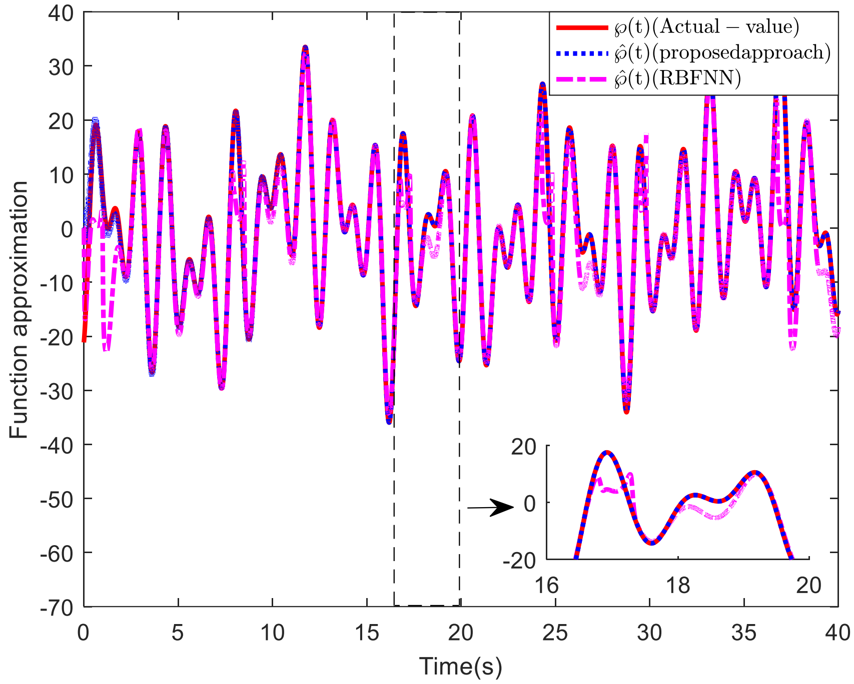

Fig. 11. Approximation of $\wp(t)$ in Test 2

distributed systems control.

Data Availability Statements

The data supporting this study's findings are available from the corresponding author upon reasonable request.

References

[1] Abdelmalak M, Benidris M and Livani H (2020, October) A polynomial chaos-based approach to quantify uncertainty of solar energy in electric power distribution systems. In 2020 IEEE/PES Transmission and Distribution Conference and Exposition (T&D): 1-5.

[2] Agrawal P N, Gupta V and Sathish Kumar A (2013) On q-analogue of Bernstein-Schurer-Stancu operators, Applied Mathematics and Computation 219: 7754-7764.

[3] Aliabadi F, Majidi M H and Khorashadizadeh S (2022) Chaos synchronization using adaptive quantum neural networks and its application in secure communication and cryptography. Neural Computing and Applications 34(8): 6521-6533.

[4] Borah M, Das D, Gayan A, et al. (2021) Control and anticontrol of chaos in fractional-order models of Diabetes, HIV, Dengue, Migraine, Parkinson's and Ebola virus diseases. Chaos, Solitons & Fractals 153: 111419.

[5] Boubellouta A, Zouari F and Boulkroune A (2019) Intelligent fuzzy controller for chaos synchronization of uncertain fractional-order chaotic systems with input nonlinearities. International Journal of General Systems 48(3): 211-234.

[6] Büyükyazıcı İ and Atakut Ç (2010) On Stancu type generalization of q-analogue of the Bernstein-Schurer-Stancu operators. Mathematical and Computer Modelling 52(5-6): 752-759.

[7] Colbaugh R, Seraji H and Glass K (1995) Adaptive compliant motion control for dexterous manipulators, Hnt. J. Robotics Research 14(3): 270-280.

[8] Corless M (1990) Guaranteed rates of exponential convergence for uncertain systems. J. Optim. Theory Appl 64(3): 481-494.

[9] Finta Z and Gupta V (2010) Approximation properties of q-analogue of the Bernstein-Schurer-Stancu operators. Central European Journal of Mathematics 8(1): 199-211.

[10] Gupta V, Mittal M and Mittal V (2021) Chaos theory and ARTFA: Emerging tools for interpreting ECG signals to diagnose cardiac arrhythmias. Wireless Personal Communications 118(4): 3615-3646.

[11] Han Z, Li S, and Liu H (2020) Composite learning sliding mode synchronization of chaotic fractional-order neural networks. Journal of Advanced Research 25: 87-96.

[12] Izadbakhsh A (2017) FAT-based robust adaptive control of electrically driven robots without velocity measurements. Nonlinear Dynamics 89: 289-304.

[13] Izadbakhsh A, Jabbari Asl H and Tatsuo Narikiyo (2019) Robust Adaptive Control of Over-Constrained Actuated Cable-Driven Parallel Robots, In: Pott A., Bruckmann T. (eds) Cable-Driven Parallel Robots. CableCon 2019. Mechanisms and Machine Science 74. Springer, Cham: 209-220

[14] Izadbakhsh A (2018) Robust adaptive control of voltage saturated flexible joint robots with experimental evaluations. AUT Journal of Modeling and Simulation 50(1) 31-38.

[15] Izadbakhsh A. and Kheirkhahan P. (2019) Adaptive Fractional-Order Control of Electrical Flexible-Joint Robots: Theory and Experiment. Proceedings of the Institution of Mechanical Engineers. Part I: Journal of Systems and Control Engineering 233(9): 1136-1145.

[16] Izadbakhsh A, Kalat AA, Khorashadizadeh S (2021) Observer-based adaptive control for HIV infection therapy using the Baskakov operator. Biomedical Signal Processing and Control 65:102343.

[17] Izadbakhsh A and Nikdel N (2021) Robust adaptive controller–observer scheme for robot manipulators: a Bernstein–Stancu approach. Robotica 40(5): 1309-1325.

[18] Izadbakhsh A (2021) An observer-based output tracking controller for electrically driven cooperative multiple manipulators with adaptive Bernstein-type approximator Robotica 40(7): 2295-2319.

[19] Izadbakhsh A, Akbarzadeh Kalat A, Fateh M M, et al. (2011) A robust anti-windup control design for electrically driven robots-Theory and Experiment. International Journal of Control, Automation, and Systems 9(5): 1005-1012.

[20] Izadbakhsh A and Rafiei S M R (2009) Endpoint perfect tracking control of robots – A robust non-inversion-based approach, International Journal of Control, Automation, and systems 7(6): 888-898.

[21] Karami H, Mobayen S, Lashkari M, et al. (2021) LMI-observer-based stabilizer for chaotic systems in the existence of a nonlinear function and perturbation, Mathematics 9(10): 1128.

[22] Kol'tsov N. I and Fedotov V K (2018) Two-Dimentional Chaos in chemical reactions. Russian Journal of Physical Chemistry B 12(3): 590-592.

[23] Li Z G, Wen C Y, Soh Y C, et al. (2001) The stabilization and synchronization of Chua's oscillators via impulsive control. IEEE Transactions on Circuits and Systems I: Fundamental Theory and Applications 48(11): 1351-1355.

[24] Mobayen S and Ma J (2018) Robust finite-time

composite nonlinear feedback control for synchronization of uncertain chaotic systems with nonlinearity and time-delay. Chaos, Solitons & Fractals 114: 46-54.

[25] Modiri A and Mobayen S (2020) Adaptive terminal sliding mode control scheme for synchronization of fractional-order uncertain chaotic systems. ISA transactions 105: 33-50.

[26] Mohammadzadeh A, Ahmadian A, Elkamel A, et al. (2021) Chaos synchronization of brushes direct current motors for electric vehicle: Adaptive fuzzy immersion and invariance approach. Transactions of the Institute of Measurement and Control 43(1): 178-193.

[27] Munmuangsaen B and Srisuchinwong B (2018) A hidden chaotic attractor in the classical Lorenz system. Chaos, Solitons & Fractals 107: 61-66.

[28] Pal P, Mukherjee V, Alemayehu H, et al. (2021) Generalized adaptive backstepping sliding mode control for synchronizing chaotic systems with uncertainties and disturbances. Mathematics and Computers in Simulation 190: 793-807.

[29] Pinzón J D and Colomé D G (2018, September) Chaos in power systems: towards short-term voltage stability analysis. In 2018 IEEE PES Transmission & Distribution Conference and Exhibition-Latin America (T&D-LA): 1-5.

[30] Priyanga P, Pattankar V V, and Sridevi S (2021) A hybrid recurrent neural network-logistic chaos-based whale optimization framework for heart disease prediction with electronic health records. Computational Intelligence 37(1): 315-343.

[31] Razmara S and Yahyazadeh M (2022) Design of an Analog Time-Varying Audio Cryptography System Based on Sliding Mode Synchronization of Non-identical Chaotic Systems Described with Time-Delayed Fractional-Order Dynamics. Arabian Journal for Science and Engineering: 1-14.

[32] Schenkendorf R, Xie X and Krewer U (2019) An efficient polynomial chaos expansion strategy for active fault identification of chemical processes. Computers & Chemical Engineering 122: 228-237.

[33] Sheikhan M, Shahnazi R and Garoucy S (2013) Synchronization of general chaotic systems using neural controllers with application to secure communication. Neural Computing and Applications 22(2): 361-373.

[34] Tai W, Teng Q, Zhou Y, et al. (2019) Chaos synchronization of stochastic reaction-diffusion time-delay neural networks via non-fragile output-feedback control. Applied Mathematics and Computation 354: 115-127.

[35] Tian K, Ren H P and Grebogi C (2019) Existence of chaos in the Chen system with linear time-delay feedback. International Journal of Bifurcation and Chaos 29(09): 1950114.

[36] Wang R, YunNing Z, Chen Y, et al. (2020) Fuzzy neural network-based chaos synchronization for a class of fractional-order chaotic systems: an adaptive sliding mode control approach. Nonlinear Dynamics 100(2): 1275-1287.

[37] Wang S, Yousefpour A, Yusuf A, et al. (2020) Synchronization of a non-equilibrium four-dimensional chaotic system using a disturbance-observer-based adaptive terminal sliding mode control method. Entropy 22(3): 271.

[38] Xu Y, Mili L, Sandu A, et al. (2018) Propagating uncertainty in power system dynamic simulations using polynomial chaos. IEEE Transactions on Power Systems 34(1): 338-348.

[39] Zhou W, Wang G, Shen Y, et al. (2018) Hidden coexisting attractors in a chaotic system without equilibrium point. International Journal of Bifurcation and Chaos 28(10): 1830033.

[40] Zhu Z Y, Zhao Z S, Zhang J, et al. (2020) Adaptive fuzzy control design for synchronization of chaotic time-delay system. Information Sciences, 535, 225-241.

Appendix A

Take a quick look; one may suppose that $\dot{e}(t)$ is utilized in (27). Here, it will be demonstrated that (27) lacks $\dot{e}(t)$. Utilizing Eq. (21), it is easy to show that:

$$\dot{\hat{\mathbf{\Lambda}}} = \mathbf{Q}^{-1}\xi(t)(-\frac{1}{\gamma}\omega(t) + \frac{\kappa_2}{\kappa_1\gamma}e(t) + \dot{e}(t)) - \sigma\mathbf{Q}^{-1}\hat{\mathbf{\Lambda}} \tag{A1}$$

Integration of (A1) gives

$$\hat{\mathbf{\Lambda}}(t) = \mathbf{Q}^{-1}\int_0^t \underbrace{\xi(\iota)}_{u}\underbrace{\dot{e}(\iota)d\iota}_{dv} + \mathbf{Q}^{-1}\int_0^t \xi(\iota)(\frac{\kappa_2}{\kappa_1\gamma}e(\iota) - \frac{1}{\gamma}\omega(\iota))d\iota - \sigma\mathbf{Q}^{-1}\int_0^t \hat{\mathbf{\Lambda}}(\iota)d\iota \tag{A2}$$

Hence, we can say:

$$\begin{aligned}\hat{\mathbf{\Lambda}}(t) = &-\mathbf{Q}^{-1}\int_0^t \dot{\xi}(\iota)e(\iota)d\iota + \mathbf{Q}^{-1}\xi(t)e(t) + \mathbf{Q}^{-1}\int_0^t \xi(\iota)(-\frac{1}{\gamma}\omega(\iota) + \frac{\kappa_2}{\kappa_1\gamma}e(\iota))d\iota \\ &-\sigma\mathbf{Q}^{-1}\int_0^t \hat{\mathbf{\Lambda}}(\iota)d\iota\end{aligned} \tag{A3}$$

Now, consider the below definition:

$$\mathbf{\Delta}(t) = -\sigma\mathbf{Q}^{-1}\int_0^t \hat{\mathbf{\Lambda}}(\iota)d\iota - \mathbf{Q}^{-1}\int_0^t \dot{\xi}(\iota)e(\iota)d\iota + \mathbf{Q}^{-1}\int_0^t \xi(\iota)(\frac{\kappa_2}{\kappa_1\gamma}e(\iota) - \frac{1}{\gamma}\omega(\iota))d\iota \tag{A4}$$

Consequently, we have

$$\begin{aligned}&\hat{\mathbf{\Lambda}}(t) = \mathbf{\Delta}(t) + \mathbf{Q}^{-1}\xi(t)e(t) \\ &\dot{\mathbf{\Delta}}(t) = \mathbf{Q}^{-1}\xi(t)(-\frac{1}{\gamma}\omega(t) + \frac{\kappa_2}{\kappa_1\gamma}e(t)) - \sigma\mathbf{Q}^{-1}\hat{\mathbf{\Lambda}}(t) - \mathbf{Q}^{-1}\dot{\xi}(t)e(t)\end{aligned} \tag{A5}$$

HOW TO CITE THIS ARTICLE
A. R. Izadbakhsh, Bernstein-Schurer-Stancu operator–based adaptive controller design for chaos synchronization in the q-analogue, AUT J. Model. Simul., 55(2) (2023) 283-298.

DOI: 10.22060/MISCJ.2024.22897.5348